AIP | Applied Physics Letters

Suppressing sub-bandgap phonon-polariton heat transfer in near-field thermophotovoltaic devices for waste heat recovery

Kaifeng Chen, Parthiban Santhanam, and Shanhui Fan

Citation: Applied Physics Letters **107**, 091106 (2015); doi: 10.1063/1.4929949
View online: http://dx.doi.org/10.1063/1.4929949
View Table of Contents: http://scitation.aip.org/content/aip/journal/apl/107/9?ver=pdfcov
Published by the AIP Publishing

Suppressing sub-bandgap phonon-polariton heat transfer in near-field thermophotovoltaic devices for waste heat recovery

Kaifeng Chen,[1] Parthiban Santhanam,[2] and Shanhui Fan[2,a)]
[1]*Department of Applied Physics, Stanford University, Stanford, California 94305, USA*
[2]*Department of Electrical Engineering, Ginzton Laboratory, Stanford University, Stanford, California 94305, USA*

(Received 8 June 2015; accepted 21 August 2015; published online 1 September 2015)

We consider a near-field thermophotovoltaic device with metal as the emitter and semiconductor as the photovoltaic cell. We show that when the cell is a III-V semiconductor, such as GaSb, parasitic phonon-polariton heat transfer reduces efficiency in the near-field regime, especially when the temperature of the emitter is not high enough. We further propose ways to avoid the phonon-polariton heat transfer by replacing the III-V semiconductor with a non-polar semiconductor such as Ge. Our work provides practical guidance on the design of near-field thermophotovoltaic systems for efficient harvesting of low-quality waste heat. © *2015 AIP Publishing LLC*.
[http://dx.doi.org/10.1063/1.4929949]

In the near field, the radiative heat transfer between two planar bodies can be significantly enhanced beyond the far-field limit as described by the Planck's law by the presence of the evanescent waves.[1–3] The application of such enhancements for thermophotovoltaics (TPV) has been widely studied.[4–9] In a standard near-field thermophotovoltaic device, a thermal emitter, typically made of a refractory metal such as Tungsten, is brought in close proximity to a photovoltaic cell which typically consists of a III-V semiconductor such as GaSb or InGaAs. Compared with far-field TPV where the thermal source is separated from the photovoltaic cell by more than a few thermal wavelengths, the use of near-field TPV is predicted to result in an enhanced power density, as well as an enhanced efficiency.[10]

In almost all previous works on near-field TPV, or TPV, in general, the intended application is to convert high temperature heat (>1000 K) to electricity. For example, for solar TPV applications, one needs to heat the emitter to a temperature of approximately 2000 K in order for the system efficiency to exceed that of a single junction solar cell.[11,12] On the other hand, there is also a critical need to develop a solid-state technology for the recovery of waste heat,[13,14] in which case the emitter is typically maintained at a much lower temperature, such as around 800 K. The analysis of a near-field TPV device for waste-heat recovery has not been done previously.

In TPV, only the photons with energy above the band gap contribute to electron-hole generation. Heat transfer as carried out by sub-band gap photons therefore is a parasitic process that is detrimental to the system efficiency. In a frequency range well below the electronic band gap, III-V semiconductors have phonon-polaritons that can contribute to such sub-band gap heat transfer. In the case of a high temperature emitter, as was previously considered, it was known that the parasitic effect from such phonon-polariton heat transfer is not substantial.[7] In this letter, we show that in TPVs designed for waste heat recovery applications, where the emitter temperature is significantly lower, the presence of phonon-polaritons can, in fact, significantly degrade system efficiency in the near field. We also show that replacing the III-V semiconductor (like GaSb) with a non-polar semiconductor (like Ge) without a sub-bandgap phonon-polariton response can be beneficial for waste-heat recovery applications.

Throughout this letter, we consider a standard configuration as shown in Fig. 1 for theoretical modeling of the near-field TPV system. The configuration consists of an emitter (body 1), usually made of refractory metal, with temperature T_1 and thickness t_1 brought into close proximity with a semiconductor photovoltaic cell (body 2) with temperature T_2 ($T_2 < T_1$) and thickness t_2. We assume $T_2 = 300$ K throughout this letter. These two bodies are separated by a vacuum gap of size d, and both bodies are backed with perfect electric conductor mirrors (Fig. 1). The photons emitted from the hot emitter are absorbed by the photovoltaic cell to generate electron-hole pairs inside the semiconductor. These electron-hole pairs can be extracted to an external circuit to generate electric power.

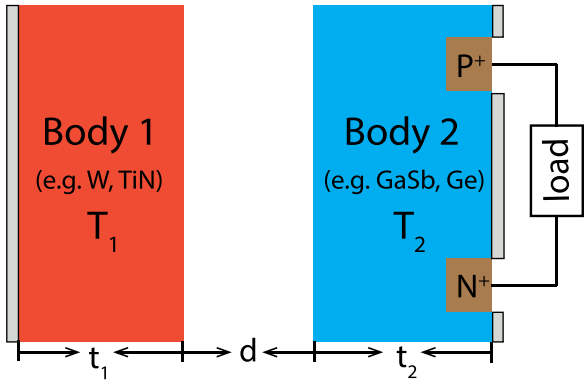

FIG. 1. Schematic of the TPV configuration. The system consists of an emitter (body 1) and a TPV cell (body 2) in close proximity. The emitters typically have high melting points, such as Tungsten and TiN, and the cell consists of a semiconductor such as GaSb and Ge.

a)shanhui@stanford.edu

We study heat transfer in this system using the formalism of fluctuational electrodynamics.[1,15] In this formalism, one describes the heat transfer between objects by computing the electromagnetic flux resulting from fluctuating current sources inside each object. The magnitude of the current fluctuation is related to the imaginary part of the dielectric function of the object. Due to reciprocity, it is sufficient to consider the current fluctuations in the photovoltaic cell. For a photovoltaic cell that employs a III-V semiconductor, its dielectric function has contributions from both the interband electronic transitions at frequencies above the band gap and from phonon-polariton excitations well below the band gap. We denote the contributions to the dielectric function from the electronic transitions and the phonon-polariton excitations as $\epsilon_e(\omega)$ and $\epsilon_p(\omega)$, respectively. The overall dielectric function is

$$\epsilon(\omega) = \begin{cases} \epsilon_e(\omega) & (\omega \geq \omega_c) \\ \epsilon_p(\omega) & (\omega < \omega_c), \end{cases} \tag{1}$$

where ω_c is the cut-off frequency chosen to separate the two different contributions mentioned above. In our calculation, we choose ω_c to be somewhat below the band gap frequency where the imaginary part of the dielectric function is near zero. The correlation functions for the current source are[16,17]

$$\langle \boldsymbol{j}_\alpha(\boldsymbol{r},\omega)\boldsymbol{j}^*_\beta(\boldsymbol{r}',\omega')\rangle \begin{cases} \frac{4}{\pi}\omega\Theta(\omega,T,V)\epsilon''_e(\omega)\delta(\boldsymbol{r}-\boldsymbol{r}')\delta(\omega-\omega')\delta_{\alpha\beta} \quad (\omega \geq \omega_c) & \text{(2a)} \\ \frac{4}{\pi}\omega\Theta(\omega,T,0)\epsilon''_p(\omega)\delta(\boldsymbol{r}-\boldsymbol{r}')\delta(\omega-\omega')\delta_{\alpha\beta} \quad (\omega < \omega_c) & \text{(2b)}, \end{cases} \tag{2}$$

where α and β label the directions of polarization, $\boldsymbol{r}$ and $\boldsymbol{r}'$ are position vectors, $\delta(\omega-\omega')$ is the Dirac delta function, $\epsilon''_e(\omega)$ and $\epsilon''_p(\omega)$ are the imaginary parts of the corresponding dielectric functions, and

$$\Theta(\omega,T,V) = \frac{\hbar\omega}{\exp\left(\frac{\hbar\omega - qV}{k_B T}\right) - 1} \tag{3}$$

is the expectation value of the photon energy in a single mode at angular frequency ω, q is the magnitude of the electron's charge, $\hbar$ is the reduced Planck's constant, k_B is the Boltzmann constant, and V is the voltage on the photovoltaic cell. Note that unlike the random current sources corresponding to electronic interband transition in Eq. (2), the magnitude of the fluctuation is independent of the cell's voltage for phonon-polariton excitations in Eq. (2).

We use the standard dyadic Green's function technique[18,19] to compute the transferred power density from the current fluctuations. Details on the dyadic Green's function can be found in Ref. 20. We compute a flux spectrum $\Phi(\omega)$ resulting from a source having fluctuation with the form $\langle \boldsymbol{j}_\alpha(\boldsymbol{r},\omega)\boldsymbol{j}^*_\beta(\boldsymbol{r}',\omega')\rangle = \frac{4}{\pi}\omega\epsilon''(\omega)\delta(\boldsymbol{r}-\boldsymbol{r}')\delta(\omega-\omega')\delta_{\alpha\beta}$. The net energy fluxes from electronic excitations E^e and phonon-polariton excitations E^p are then obtained by integrating over the appropriate frequency ranges

$$E^e = \int_{\omega_c}^{+\infty} [\Theta(\omega,T_1,0) - \Theta(\omega,T_2,V)]\Phi(\omega)\,d\omega, \tag{4}$$

$$E^p = \int_0^{\omega_c} [\Theta(\omega,T_1,0) - \Theta(\omega,T_2,0)]\Phi(\omega)\,d\omega. \tag{5}$$

A similar calculation also yields the net above-band-gap photon flux between the two bodies as

$$F = \int_{\omega_c}^{+\infty} \frac{[\Theta(\omega,T_1,0) - \Theta(\omega,T_2,V)]}{\hbar\omega}\Phi(\omega)\,d\omega. \tag{6}$$

We combine the fluctuational electrodynamic calculations with a detailed balance analysis of the photovoltaic cell[21] to analyze the TPV system. At a given voltage V on the photovoltaic cell, the current density J passing through the cell can be written as

$$J = q\,(F - R), \tag{7}$$

where F and R represent the generation rate of electron-hole pairs and nonradiative recombination rate, respectively, per unit area of the TPV cell. F depends on the voltage V as shown in Eq. (6). In this paper, for nonradiative recombination, we only consider the Auger process, which dominates in high-quality materials, and set R in Eq. (7) to[22]

$$R = (C_n n + C_p p)(np - n_i^2)t_2, \tag{8}$$

where n and p are the electron and hole concentrations, respectively, t_2 is the thickness of the cell, and n_i is the intrinsic carrier density. Having computed the current density through the cell, we then obtain the output electric power density and the efficiency of this near-field TPV system as

$$P = JV, \tag{9}$$

$$\eta = \frac{P}{E^e + E^p} \times 100\%, \tag{10}$$

where $E^e + E^p$ is the net energy flux from the emitter to the cell. To obtain either the maximum power or the maximum efficiency, we use either Eq. (9) or (10) and maximize with respect to voltage. In general, the voltages required to achieve maximum power differ from those for maximum efficiency. We note that this calculation directly incorporates the effect of photon-recycling between the emitter and the cell.

Throughout this letter, we choose Tungsten (W) as the emitter. We assume GaSb and Ge as the materials for the TPV cell. In the calculation, t_1 is chosen to be 1 μm to ensure

significant emission from the Tungsten, t_2 is optimized to be 1 μm, which gives high efficiency when the separation between the emitter and the cell is in the far-field regime. In the case of a GaSb cell at $T_2 = 300$ K, GaSb has a band gap of 0.726 eV, intrinsic carrier density $n_i = 1.5 \times 10^{12}\,\mathrm{cm}^{-3}$, and Auger recombination coefficient $C_0 = C_n + C_p = 5 \times 10^{-30}\,\mathrm{cm}^6\,\mathrm{s}^{-1}$.[23] In Eqs. (2a) and (2b), we choose $\hbar\omega_c = 0.6$ eV, below which the contribution to the photon emission from interband process is negligible. In the case of a Ge cell, Ge has a band gap of 0.66 eV, intrinsic carrier density $n_i = 2 \times 10^{13}\,\mathrm{cm}^{-3}$, and Auger recombination coefficient $C_0 = C_n + C_p = 1 \times 10^{-30}$ cm^6 s^{-1}.[23] In the calculation, we choose $\hbar\omega_c = 0.64$ eV, below which the absorption from Ge is very weak and is ignored in our calculations. The dielectric functions $\epsilon_e(\omega)$ and $\epsilon_p(\omega)$ for GaSb are obtained from Refs. 24 and 25, and those for W and Ge are from Ref. 24. For GaSb, its tabulated dielectric function $\epsilon_p(\omega)$ is well accounted for by the phonon-polariton model, which gives a dielectric function of $\epsilon_p(\omega) = \epsilon_\infty(\omega^2 - \omega_L^2 + i\gamma\omega)/(\omega^2 - \omega_T^2 + i\gamma\omega)$, where ω_T and ω_L correspond to energies of 0.0286, 0.0298 eV, respectively, $\epsilon_\infty = 14.63$, and $\gamma = 3.3514 \times 10^{11}$ rad/s.

We apply the formalisms as described above to the TPV systems shown in Fig. 1. We consider W-GaSb system first. In Figs. 2(a) and 2(b), we show the maximum system efficiency and the maximal electric power density, respectively, as a function of gap size d for the W-GaSb system. At a high emitter temperature $T_1 = 2000$ K, the system has an efficiency of 56% in the near-field region at $d = 10$ nm, as compared to an efficiency of 54% in the far-field region at $d = 10\,\mu$m [Fig. 2(a), purple curve]. Also, the maximum electric power density increases from $5.67 \times 10^4\,\mathrm{W/m}^2$ at $d = 10\,\mu$m to $1.66 \times 10^6\,\mathrm{W/m}^2$ at $d = 10$ nm. Therefore for W-GaSb system with $T_1 = 2000$ K, operating in the near-field results in the increase of both the system efficiency and the maximal electric power density. Here, the increase of the maximal electric power density in the near-field arises from the enhancement of heat transfer in the near field. The improvement of efficiency of near field results from narrowing of the thermal emission spectrum[4–6] in the near-field due to the plasmons in Tungsten.

For waste heat recovery, the emitter usually has relatively lower temperatures. In Figs. 2(a) and 2(b), we present the efficiency and the power density for $T_1 = 800$ K in the green curves. Similar to the case of high-temperature emitter, we still observe a power density increase from 24.7 W/m^2 at $d = 10\,\mu$m to 839.5 W/m^2 at $d = 10$ nm. However, unlike the case of a high-temperature emitter, here the system efficiency decreases in the near-field regime. The system has an efficiency of 50% in the far-field region with $d = 10\,\mu$m, as compared to an efficiency of only 39% in the near-field region with $d = 10$ nm.

To understand the different efficiency behaviors for the W-GaSb system at different emitter temperatures, we plot in Figs. 3(a) and 3(b) the net heat transfer spectra at various gap sizes, for $T_1 = 2000$ K and 800 K, respectively. The heat transfer spectra due to electron and phonon-polariton excitations correspond to the integrands in Eqs. (4) and (5), respectively, with $V = 0$. The heat transfer spectra are significant only in the frequency range where GaSb has significant absorption. This is a distinct signature of photon-recycling between the emitter and the photovoltaic cell: Photons from the emitter that are not absorbed by the PV cell are reflected back to the emitter. As a result, photon recycling naturally achieves the narrowing of the heat transfer spectrum that is quite desirable for TPV applications.

In Figs. 3(a) and 3(b), the sharp spectral peaks (red curves) arise from the phonon-polariton excitations. The phonon-polariton resonance corresponds to a wavelength of 42 μm. Since all the three gap sizes chosen here ($d = 10$ nm, 1 μm, and 10 μm) are significantly smaller than the phonon-polariton wavelength, the system is in the near-field regime for all these three gap sizes. The height of the spectral peaks increases dramatically as one goes from $d = 10\,\mu$m to $d = 10$ nm, indicating very significant enhancements of heat transfer in the near field.

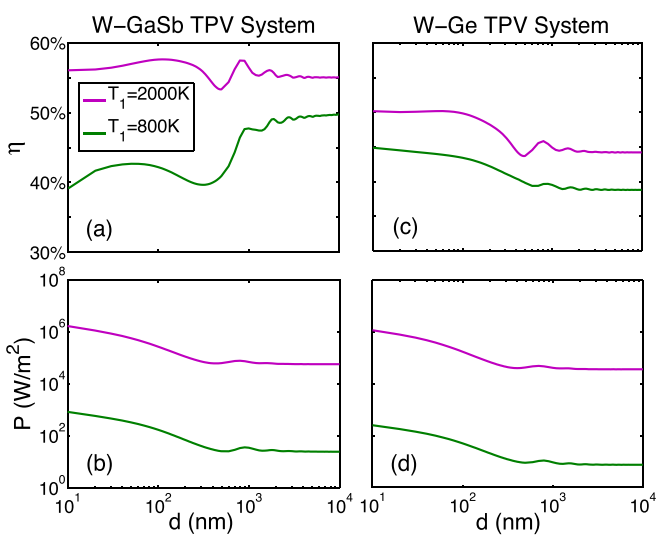

FIG. 2. Efficiencies and electric power densities for the W-GaSb [(a) and (b)] and W-Ge TPV systems [(c) and (d)] as a function of the gap size d. Results for $T_1 = 2000$ K and $T_1 = 800$ K are plotted in purple and green curves, respectively.

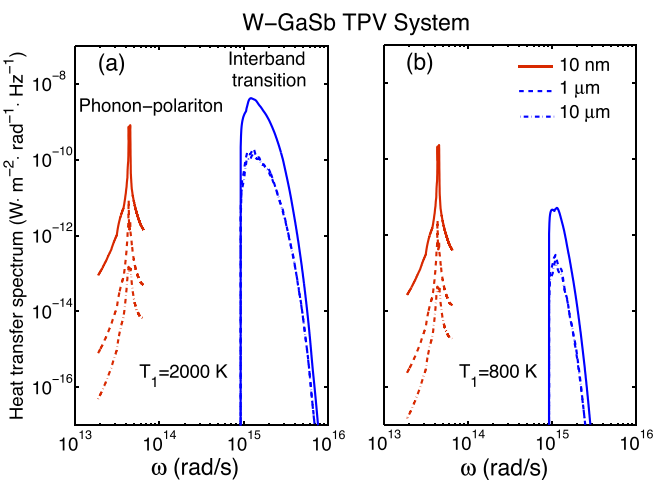

FIG. 3. The flux spectra for interband transitions and phonon-polaritons excitations in blue and red, respectively, at $T_1 = 2000$ K (a) and $T_1 = 800$ K (b) for various gap separations in W-GaSb TPV system. The mechanism of the two spectra, i.e., phonon-polariton in red and interband transition in blue, is clearly labeled in the figures. The solid curves, dashed curves, and dotted curves correspond to $d = 10$ nm, 1 μm, and 10 μm, respectively. Both the spectra and the angular frequency are plotted in log scale.

In Figs. 3(a) and 3(b), the broad spectra plateaus (blue curves) are due to electronic excitations. The lower cut-off frequency of the plateaus for both emitter temperatures remains constant around the band gap frequency $\omega_g = 1.1 \times 10^{15}$ rad/s of GaSb. The width of plateaus is approximately $k_B T_1$ since the net heat transfer is dominated by the emission of Tungsten.

The band gap of GaSb corresponds to a wavelength of 1.7 μm. Thus, the system is in the far-field regime with $d = 10\,\mu$m and is starting to enter the near-field regime with $d = 1\,\mu$m. The spectral plateaus for these two gap sizes (blue dashed and dashed-dotted lines in Fig. 3) therefore approximately overlap, since in the far field the heat transfer is independent of the gap size. As one further reduces the gap size to $d = 10$ nm, the heights of the plateaus increase dramatically due to the enhanced heat transfer in the near field.

At $T_1 = 2000$ K [Fig. 3(a)], we see that the heat transfer due to the electronic excitations (blue curves) significantly dominates over that due to the phonon-polaritons for all gap sizes. In contrast, at $T_1 = 800$ K [Fig. 3(b)], the contributions of phonon-polaritons to the heat transfer become significant in the near field. To further illustrate this point, we plot the spectrally integrated heat transfer power density due to electronic excitation (E^e in Eq. (4) with $V = 0$) and phonon-polariton (E^p in Eq. (5)) as a function of gap size d in Fig. 4. At $T_1 = 2000$ K, the heat transfer from the electronic excitation dominates that from the phonon-polariton by several orders of magnitude for all gap sizes [Fig. 4(a)]. As a result, phonon-polariton does not play a significant role at such elevated emitter temperature. Both the system efficiency and the electric power density improve as one reduces the gap size to the near-field region [Fig. 2(a)]. In contrast, at lower emitter temperature of $T_1 = 800$ K, the electronic excitation has a contribution that is more than two-orders of magnitude larger than that of the phonon-polariton in the far field, but only a factor of 2 larger as d reduces to 10 nm. As a result, the phonon-polariton plays a significant role in the near field. The system efficiency degrades significantly as the gap size decreases as shown in Fig. 2(a). Our observation here, that from efficiency consideration, in TPV one needs to eliminate sub-band gap absorption and emission, and hence for waste-heat recovery one needs to eliminate phonon-polariton contribution, is consistent with the conclusion of Ref. 26 that discussed the theoretical condition for ideal near-field TPV systems. In the W-GaSb system, the phonon-polariton plays a negligible role in the far-field regime, and hence does not affect the system efficiency for the far-field TPV system.

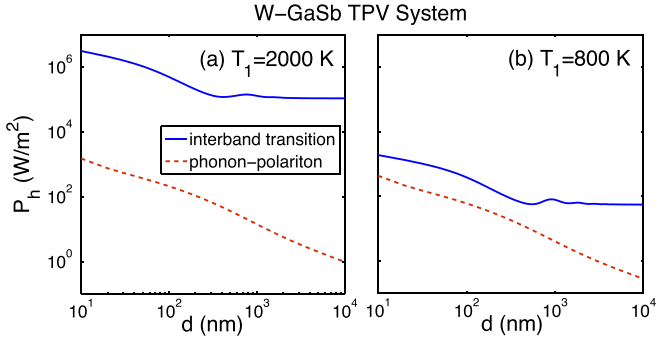

FIG. 4. Net heat transfer power density P_h for W-GaSb TPV system from interband transitions (blue solid curves) and phonon-polariton excitations (red dashed curves) as a function of gap separation for $T_1 = 2000$ K (a) and $T_1 = 800$ K (b), respectively. The gap separation d ranges from 10 nm to 10 μm and is plotted in log scale.

In TPV applications, the available power density decreases rapidly as one reduces the emitter temperature. For waste heat recovery, since the emitter is typically at a much lower temperature, the capability to use the near field to enhance the electric power density is therefore particularly attractive. To overcome the efficiency deterioration in the near field as discussed above, we consider the use of a Ge photovoltaic cell. Since Ge is non-polar, it does not have a phonon-polariton response. For the Ge system, both the system efficiency and the electric power density improve as one reduces the gap size, as shown in Figs. 2(c) and 2(d).

In summary, in this letter, we have shown that the parasitic phonon-polariton heat transfer that can occur in a conventional TPV system which utilizes a III-V semiconductor cell has detrimental effect on the system efficiency, especially when the emitter has a relatively low temperature. We further propose avoiding this outcome by choosing a non-polar cell material. Our work points to the important opportunities of operating TPV device in the near field for waste heat recovery.

This work was supported by the DOE "Light-Material Interactions in Energy Conversion" Energy Frontier Research Center under Grant No. DE-SC0001293.

[1]D. Polder and M. Van Hove, Phys. Rev. B **4**, 3303 (1971).
[2]J. B. Pendry, J. Phys.: Condens. Matter **11**, 6621 (1999).
[3]J. J. Loomis and H. J. Maris, Phys. Rev. B **50**, 18517 (1994).
[4]A. Narayanaswamy and G. Chen, Appl. Phys. Lett. **82**, 3544 (2003).
[5]M. Laroche, R. Carminati, and J.-J. Greffet, J. Appl. Phys. **100**, 063704 (2006).
[6]S. Basu, Z. M. Zhang, and C. J. Fu, Int. J. Energy Res. **33**, 1203 (2009).
[7]M. Francoeur, R. Vaillon, and M. Menguc, IEEE Trans. Energy Convers. **26**, 686 (2011).
[8]K. Park, S. Basu, W. King, and Z. Zhang, J. Quant. Spectrosc. Radiat. Transfer **109**, 305 (2008).
[9]S. Basu, Y.-B. Chen, and Z. M. Zhang, Int. J. Energy Res. **31**, 689 (2007).
[10]A. V. Shchegrov, K. Joulain, R. Carminati, and J.-J. Greffet, Phys. Rev. Lett. **85**, 1548 (2000).
[11]N.-P. Harder and P. Würfel, Semicond. Sci. Technol. **18**, S151 (2003).
[12]E. Rephaeli and S. Fan, Opt. Express **17**, 15145 (2009).
[13]L. E. Bell, Science **321**, 1457 (2008).
[14]B. Heeg, J.-B. Wang, S. R. Johnson, B. D. Buckner, and Y.-H. Zhang, Proc. SPIE **6461**, 64610K (2007).
[15]S. M. Rytov, *Theory of Electric Fluctuations and Thermal Radiation* (Air Force Cambridge Research Center, Bedford, MA, 1959).
[16]C. H. Henry and R. F. Kazarinov, Rev. Mod. Phys. **68**, 801 (1996).
[17]K. Chen, P. Santhanam, S. Sandhu, L. Zhu, and S. Fan, Phys. Rev. B **91**, 134301 (2015).
[18]M. Krüger, T. Emig, and M. Kardar, Phys. Rev. Lett. **106**, 210404 (2011).
[19]C. R. Otey and S. Fan, Phys. Rev. B **84**, 245431 (2011).
[20]W. C. Chew, *Waves and Fields in Inhomogeneous Media* (IEEE, New York, 1995).
[21]W. Shockley and H. J. Queisser, J. Appl. Phys. **32**, 510 (1961).
[22]O. Heikkilä, J. Oksanen, and J. Tulkki, J. Appl. Phys. **105**, 093119 (2009).
[23]I. P.-T. Institute, "NSM Archive - Physical Properties of Semiconductors," (1998).
[24]E. Palik, *Handbook of Optical Constants of Solids* (Academic, New York, 1985).
[25]R. Ferrini, M. Patrini, and S. Franchi, J. Appl. Phys. **84**, 4517 (1998).
[26]S. Molesky and Z. Jacob, Phys. Rev. B **91**, 205435 (2015).